Hindawi
Wireless Communications and Mobile Computing
Volume 2018, Article ID 8920746, 10 pages
https://doi.org/10.1155/2018/8920746

Research Article

A Multiple-Access Time and Frequency Spectrum-Spreading Modulation

Samer S. Saab, Joe Khalife, and Rayana H. Jaafar

Department of Electrical and Computer Engineering, Lebanese American University, Byblos, Lebanon

Correspondence should be addressed to Samer S. Saab; ssaab@lau.edu.lb

Received 13 June 2018; Revised 30 September 2018; Accepted 8 October 2018; Published 25 October 2018

Academic Editor: André de Almeida

In this paper a novel modulation scheme called Carrier Interleaved Multiple Access (CIMA) is proposed. CIMA provides an alternative for multiple-access modulation accommodating resistance to noise and channel interference. The approach is based on polar signaling modulated with an FM-like composite sinusoidal function. The user assigned frequency deviation and modulation index are strictly related and unique. The latter parameters are generated using a nontraditional pseudorandom noise generator (PRNG). This PRNG provides CIMA with low interference capability between cochannels and adjacent channels. CIMA can be considered for a single-user or multiple-access technique. Selected CIMA characteristics are presented. In order to numerically illustrate the effectiveness of the proposed modulation scheme, the performance of CIMA is compared with the conventional direct-sequence spread spectrum binary phase-shift keying (DSSS-BPSK) modulation.

1. Introduction

Wireless communications connect more devices than people and the trend is only increasing in both venues. The number of connected devices per person rose to 1.84 in 2010 [1], and it is expected that we will have seven trillion devices connected wirelessly by 2020 [2]. Over the past ten years smartphones and tablet PCs resulted in a significant increase in the number of devices connected to the internet. However, other prospective wireless applications such as vehicle-to-vehicle communication, applications based on the use of radio frequency identification (RFID), wireless electric meters, and other applications not yet envisaged may evolve. Consequently, an increase in investigation activities towards various and novel wireless communication schemes associated with different applications is desired. Common characteristics for wireless communication systems remain to include spectral efficiency, security, and interference resistance.

Spread spectrum techniques are employed for secure communications, increasing resistance to interference, noise, and jamming. Different techniques of spread spectrum include frequency-hopping spread spectrum (FHSS), direct-sequence spread spectrum (DSSS), time-hopping spread spectrum (THSS), chirp spread spectrum (CSS), and in some cases combinations of these forms. For example, in Multicarrier Direct-Sequence CDMA (MC-DS-CDMA) time and frequency spreading is used [3]; also lattice reduction theory and aided multiple user detection is applied to a spread spectrum system leading to near-far effect suppression [4]. A conventional spread spectrum system employs pseudo-noise (PN) code generators while other schemes employ nondeterministic spreading codes generated from a random input data stream such as the self-encoded spread spectrum (SESS) [5].

Ultra-wideband (UWB) is another modulation technique [6] that possesses similar characteristics to spread spectrum. It is based on transmitting short duration pulses and is applied to short-range wireless communication. In order to improve its performance, DSSS techniques have been introduced to UWB systems [7]. Another technique is the chaotic communication where a noise-like, aperiodic, chaotic signal is employed to modulate the information signal. Different chaos modulation techniques have been proposed (see, e.g., [8, 9] and references therein). In Differential Chaos Shift Keying (DCSK), index modulation is integrated to improve the system's data rate and energy efficiency such as permutation index DCSK (PI-DCSK) [10] and Commutation Code Index DCSK (CCI-DCSK) [11]. Recently, Code Index

Modulation (CIM) has been proposed for spread spectrum systems [12]. In CIM, the indices of spreading codes are used in conjunction with symbol constellation for bits mapping. The latter scheme aims to achieve high data rate communication without sacrificing system complexity and energy requirement. In noncoherent multicarrier spread spectrum systems, the reference signal is sent once for multiple parallel bits yielding significant energy savings and a higher spectral efficiency as compared to other DSCK systems. Other methods employing efficient coding techniques aimed at reducing energy costs, i.e., memory and processing cost, in standard spread spectrum (SS) communication systems [13]. Continuous phase modulation combined with DSSS is proposed in [14] and further investigated in [15–18]. Recently, index modulation has been applied to a coherent chaos-based scheme where the initial conditions of the chaotic sequence are used as a new dimension to map information and carry extra bits [19]. All the proposed modulation methods above come with a number of unique features.

Siding away from spread spectrum techniques, the relatively new spatial-shift keying (SSK), which is widely implemented for multiple-input multiple-output (MIMO) systems, is considered as a strong candidate for next generation wireless communication systems [20]. The same applies for orthogonal frequency division multiplexing (OFDM), which is believed to be the best in multicarrier modulation and is also extensively used in broadband and MIMO systems [21]. However, multicarrier OFDM and even single-carrier OFDM have some drawbacks [21]. For example, due to leakage of the FFT, OFDM is more sensitive to carrier frequency offset and drift than single-carrier systems, the need of high peak-to-average-power ratio [22], and sensitivity due channel spatial correlation. In [23], a frequency index modulation scheme is proposed to reduce peak-to-average-power ratio of OFDM systems without sacrificing data rate.

The commonly pseudorandom sequences used in communication systems are maximal length sequences [24], Mersenne Twister code, Walsh sequences, and Gold codes [25], Kasami codes [26], and Barker codes [27]. In order to improve the spectral efficiency in MIMO systems, space-time block codes [28, 29] and space-time trellis codes are employed. However, none of the communication systems employs the nontraditional pseudorandom noise generator (PRNG) proposed in [30]. The latter is based on a linear combination of continuous-time composite sinusoidal signals. The desired signals' key parameters are easily constructed by choosing a set of prime numbers with bounds depending on the typical requirements of the PRNG [30]. The key characteristics of the PRNG are as follows: The period of the signal can be made arbitrarily large, at least 98% of the signal total average power is contained in the desired frequency bandwidth, a desired bandwidth can be arbitrarily selected, and the cross-correlation between any pair of generated signals can be made arbitrarily small. This answers concerns on interchannel interference raised by many researches on spread spectrum techniques, such as in FHSS [31].

In this paper, a new modulation scheme, named CIMA, is proposed. In DSSS, there is a fast phase shift of 180° through a predefined sequence known to both the receiver and the transmitter. In FHSS, there is a fast hopping of the signal into different frequencies. The set of frequencies is also known to both the receiver and the transmitter. In CIMA, instead of having a discrete phase shift or frequency shift like DSSS or FHSS, we have both phase and frequency change in the form of a predefined composite sinusoidal function known to both the receiver and the transmitter. CIMA modulator is formed by multiplying a bipolar digital message signal with $\cos(2\pi f_c t + \beta_m \sin(2\pi f_m t))$, where each message signal is associated with a unique signature pair (β_m, f_m). The choice of β_m and f_m is the key in rejecting cochannel interference, which is an essential cause of the signal's quality degradation and capacity constraint in wireless mobile telephony and other applications. The proposed PRNG in [30] is employed for generating different pairs (β_m, f_m). Each pair is strictly correlated and all different pairs are made weakly correlated but equally constrained to a bandwidth measure.

This proposed method can be used as a single-user or a multiple-access technique. Due to the composite sinusoidal function employed at the modulator, the sinc functions corresponding to the polar signaling are spread around the carrier within the same channel with frequency separation of nf_m, $n = 0, \pm 1, \pm 2, \ldots, \pm\beta_m + 1$. In multiple-access application, each user is assigned different (β_m, f_m). Consequently, all the sinc functions associated with different users are separated by different values of f_m, which are all situated around the carrier within the same channel and the instantaneous frequency of a CIMA signal is given by $f_{inst}(t) = f_c + f_m\beta_m\cos(2\pi f_m t))$. This type of spectral interleaving around the carrier awards "Carrier Interleaved Multiple Access" terminology. CIMA aims at rejecting adjacent and cochannel interference.

The characteristics of the proposed modulation scheme are analytically presented including bandwidth analysis, bit error rate (BER) due to channel noise, and cochannel and adjacent channel interference. Numerical simulations examine the performance of the proposed scheme contrasted with DSSS-BPSK while considering a more complex channel model.

The rest of this paper is organized as follows. Section 2 describes the proposed CIMA system and the employed PRNG, and it presents relevant parameters and new characteristics of the PRNG. Section 3 contains analytical analysis describing CIMA characteristics. Section 4 includes a comparative study with DSSS-BPSK scheme based on numerical simulations, and finally Section 5 contains conclusions and future work.

2. Proposed System Model

In this section we present the basics of CIMA modulation and demodulation and the employed PRNG algorithm and establish some preliminary new results relevant to the employed PRNG.

2.1. System Transmitter and Receiver. At the transmitter side, the j^{th} message signal, $m_j(t)$, is assumed to be in the form of polar digital signaling with a bit rate R, where $R = 1/T_b$

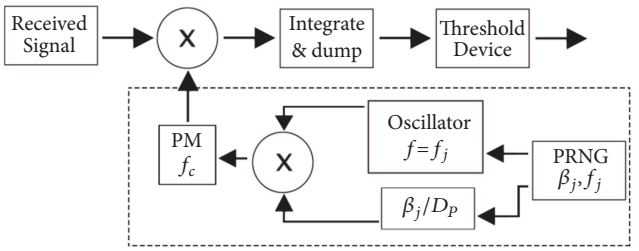

Figure 1: Proposed CIMA receiver.

and T_b is the time it takes to send 1 bit of data. The proposed modulator has the following form:

$$y_j(t) = Am_j(t)\cos\left(2\pi f_c t + \beta_j \sin\left(2\pi f_j t\right)\right), \quad 1 \le j \le L, \tag{1}$$

where L is the number of multiple users, f_c is the carrier frequency, and β_j and f_j are two parameters, which are chosen according to the PRNG algorithm [30] and A is any nonzero real number included to specify the power level.

It is important to note that (1) is somehow similar to both DSSS and FHSS. Unlike FHSS where the transmitted signal rapidly switches its carrier among many frequency channels within a bandwidth, B_y, CIMA (1) spreads its signal within B_y continuously according to the PRNG presented in [30]. CIMA makes the resulting wideband signal appear as a noise signal. It is that the specific spreading associated with PRNG signal gives much more freedom than the conventional spread spectrum techniques.

An analog platform for generating the composite sinusoidal signal, $\cos(2\pi f_c t+\beta_j \sin(2\pi f_j t))$, is shown in the dashed box of Figure 1. The constant D_P is the phase sensitivity of the phase modulator (PM). Figure 1 presents one platform for a CIMA receiver. The transmitter consists of a multiplier that multiplies the polar data signal, $m_j(t)$, with the same composite sinusoidal signal used in the receiver, where it is assumed that the parameters β_j and f_j are known to both the receiver and the transmitter.

Implementation remarks on generating the PRNG signals [30]: Depending on the specific application, the user should select the appropriate platform. For example, if numerical simulations (e.g., Monte Carlo simulations) are intended, then a PC-based platform can be used in a non-real-time fashion. However, for real-time application, the choice of platform becomes essential. For example, if the PRNG is intended to be used in an analog platform, then the PRNG signal can be generated by using a voltage-controlled oscillator. However, for real-time digital applications, a DSP platform with moderate memory size can be considered. However, in case of applications where L is large then the FPGA platform can be advantageous over the DSP platform for its superiority in handling parallel processing execution. The limitation depends on the size of L, f_c, B, the processor speed, and processor architecture. The complexity of the proposed algorithm becomes $O(n)$. That is, we have a linear algorithm with a performance $c \times n$ where c is the cost of one run and n is the size of the input.

2.2. PRNG Algorithm. This section presents a special case of the PRNG algorithm proposed in [30] that is employed by CIMA. It also establishes results that are essential for studying some of the characteristics of the proposed modulation scheme.

The j^{th} PRNG signal, as presented in [27], is given by

$$x_j(t) = A_j \sum_{i=1}^{N} \cos\left(2\pi f_c t + \beta_{i,j} \sin\left(2\pi f_{i,j} t\right)\right), \quad 1 \le j \le L, \tag{2}$$

where L is the number of feasible generated signals and N is the number of composite sinusoidal signals. It is important to note that as N is increased, the period of the PRNG signal becomes larger and its spectrum becomes flatter within its bandpass centered at f_c. A larger value of N is intended for band jamming application. Consequently, in this paper, we consider a special case of (2) with $N = 1$, and set $A_j \equiv A$, for all j. Therefore, we omit the index i from the equation, to obtain the unmodulated CIMA signal presented in the following form:

$$x_j(t) = A\cos\left(2\pi f_c t + \beta_j \sin\left(2\pi f_j t\right)\right). \tag{3}$$

The power spectral density (PSD) of $x(t)$ is given by [28]:

$$P_{x_j}(f) = \frac{A^2}{4} \sum_{n=-\infty}^{\infty} J_n^2\left(\beta_j\right) \cdot \left[\delta\left(f - f_c - nf_j\right) + \delta\left(f + f_c + nf_j\right)\right], \tag{4}$$

where $J_n(\beta_j)$ represents the Bessel function of the first kind of order n and argument β_j. The carrier frequency is f_c and the single-sided bandwidth of the unmodulated signal, $x_j(t)$, is $B = 2(\beta_j + 1)f_j$, $\beta_j > 1$, where at least 98% of the total average power of each signal is contained in the bandwidth B. The parameters (the weak correlation among the pairs (f_j, β_j) is illustrated in Corollary 1 and Theorem 1 of [30]) of the proposed PRNG are constructed as follows [30]:

$$f_j = \frac{p_j}{l} = \frac{B}{2\left(\beta_j + 1\right)}, \quad 1 \le j \le L. \tag{5}$$

Or $\beta_j = lB/2p_j - 1$, where l is a positive real number that depends on L and p_j is any prime number such that

(1) $p_j \ne l$, for all j

(2) $p_j \ne B$ for all j

(3) $p_{\min} \equiv \min(p_j) \ge Rl > e$, $1 \le j \le L$

(4) $p_{\max} \equiv \max(p_j) \le Bl/2(\beta_{\min} + 1)$, $1 \le j \le L$

In order to guarantee that $p_{\max} > p_{\min}$, then B should be significantly larger than $2(\beta_{\min} + 1)R$, which leads to $f_j > R$, $1 \le j \le L$.

Depending on the upper and lower bound of p_j, the proposed algorithm can generate L continuous-time cochannel signals, $x_j(t)$, $1 \le j \le L$. Since $f_j = p_j/l$, then setting $\min_j(p_j) = lR$ guarantees $\min_j(f_j) > R$. When $\beta_{\min}$ is notably larger than one, then the upper bound of p_j guarantees that at least 98% of the total average power of each signal is contained in the bandwidth B. Since the bandwidth B is much larger than R, we refer to B as the spread bandwidth.

In what follows we introduce two CIMA-relevant parameters γ and α that are directly related to the spread bandwidth B and the number of signals L. We express B in terms of the bit rate R; in particular, $B \equiv \alpha R$, where $\alpha > 2(\beta_{\min} + 1)$, and we express L in function of α and γ, $L \equiv \gamma\alpha$, where $\gamma > 0$. In fact, α is considered as the spreading factor and γ, for $\alpha \gg 1$, the spectral efficiency. The value of γ is elaborated in (11).

In the next section, we show that the null-to-null bandwidth of $y_j(t) \approx (\alpha + 2)R$. For example, if $\alpha = 100$ and $\gamma = 1.3$, then 130 CIMA signals can share a common channel with bandwidth equal to $102R$.

Remark 1. In multiple-access applications of the proposed modulation scheme, the desired number of cochannel signals, L, is specified. Proposition A.2 (see Appendix) indicates that L increases if and only if l increases. However, since how to obtain meaningful analytical formulation for l in function of the relevant parameters is not clear, l is obtained numerically (see Appendix).

Remark 2. The spacing between two consecutive frequencies is given by

$$\Delta f_j \equiv f_j - f_{j-1} = \frac{p_j - p_{j-1}}{l} \ge \frac{2}{l}. \tag{6}$$

Therefore, as L increases, l increases and Δf_j decreases. Based on Monte Carlo simulations, while considering $\{f_j\}$ being an ordered set of increasing values, the following approximations are obtained:

$$\begin{aligned} \min_{2\le j\le L}\left(\left|f_j - f_{j-1}\right|\right) &= \frac{2}{l} \approx 0.1\frac{R}{\gamma} \\ \min_{3\le j\le L}\left(\left|f_j - f_{j-2}\right|\right) &\approx 0.3\frac{R}{\gamma}. \end{aligned} \tag{7}$$

In addition, $\min_{m+1\le j\le L}(|f_j - f_{j-m}|)$ significantly increases as m increases.

Lemma 3. *For fixed values of γ and α where $\alpha > 2(\beta_{\min} + 1)$ and $\gamma > 0$, the product $R \times l$ is equal to a positive constant.*

The proof of Lemma 3 is provided in Appendix along with other novel and relevant results. Lemma 3 helps in establishing basic characteristics pertaining to CIMA.

3. CIMA Characteristics

In this section, we analytically present the PSD and bandwidth of a CIMA signal, spectral efficiency, and the bit error rate (BER) due to channel noise. In addition, we study the cochannel interference rejection capability of the proposed scheme.

3.1. PSD, Bandwidth, and Spectral Efficiency. The PSD of a CIMA signal is first derived. Consider

$$x(t) = A\cos\left(2\pi f_c t + \beta_m \sin\left(2\pi f_m t\right)\right) \tag{8}$$

and consider a polar nonreturn-to-zero (NRZ) signal denoted by $m(t)$ to be the baseband polar signal represented by $m(t) = \sum_{n=-\infty}^{n=\infty} a_n z(t - nT_b)$, where $z(t) = rect(t/T_b)$.

It is assumed that the values of a_n are equally likely to occur, the data are independent, and, for simplicity, the possible levels for a_n's are ± 1. The modulated signal is $y(t) = m(t)x(t)$. It can be shown that the PSD of $z(t)$ is given by $\mathscr{P}_z(f) = T_b \mathrm{sinc}^2(T_b f)$ and the PSD of $y(t)$ is given by

$$\begin{aligned} \mathscr{P}_y(f) = \frac{A^2 T_b}{2} &\sum_{n=-\infty}^{\infty} J_n^2(\beta_m) \\ &\cdot \left[\mathrm{sinc}^2\left(T_b\left(f - f_c - nf_m\right)\right)\right. \\ &\left. + \mathrm{sinc}^2\left(T_b\left(f + f_c + nf_m\right)\right)\right]. \end{aligned} \tag{9}$$

Therefore, the PSD of the signal consists of shifted versions of $\mathrm{sinc}^2(\cdot)$ functions weighted by the Bessel functions, $J_n^2(\beta_m)$. Consequently, the single-sided "null-to-null" bandwidth of $m(t)$, B_y, is

$$B_y \cong B + 2R = (\alpha + 2)R. \tag{10}$$

When $\alpha \gg 1$, then $B_y \cong B = \alpha R$. Therefore, a channel with bandwidth $= B_y$ can accommodate $L = \gamma\alpha$ different signals. Note that the above equation assumes that the data used is not prefiltered and has the polar NRZ form. If the message signal is prefiltered, for example, by using a Gaussian filter, the bandwidth occupied by the signal will become smaller and the performance due to adjacent channel interference (ACI) will be improved.

The spectral efficiency is defined as $\eta_L \equiv LR/B_y$, which leads to

$$\eta_L = \frac{LR}{B_y} = \frac{\gamma\alpha}{\alpha + 2} \cong \gamma\big|_{\alpha\gg 1}. \tag{11}$$

3.2. Bit Error Rate due to Channel Noise. The BER is derived for the proposed scheme due to white Gaussian channel noise. Derivations assume that the receiver is based on coherent detection incorporating a multiplier and a matched filter as illustrated in Figure 1. In addition, it is assumed that the CIMA signal $y(t)$ plus white Gaussian noise $n(t)$ (over the equivalent bandpass) is present at the input of the matched filter. The PSD of $n(t)$ over the equivalent bandpass is $N_0/2$.

Since the CIMA scheme is based on coherent reception, then it can be shown that the probability of error (or BER) for matched-filter reception with an optimum threshold is given by $P_e = Q(\sqrt{E_d/2N_0})$, where $Q(z) = (1/\sqrt{2\pi})\int_z^\infty e^{-\xi^2/2}d\xi$ and E_d is the difference signal energy at the receiver input. Since for all practical purposes $f_c \gg 1/T_b$, then $E_d \cong 2A^2T_b$. The average energy per bit becomes $E_b \cong A^2T_b/2$. Therefore, the BER is $P_e \cong Q(\sqrt{A^2T_b/N_0}) = Q(\sqrt{2E_b/N_0})$, which is similar to the BER corresponding to BPSK.

3.3. Cochannel Interference (CCI). In what follows, the cochannel interference of the proposed CIMA system in terms of its capability of partially rejecting other CIMA cochannel signals is analyzed both in the time domain and then in the frequency domain.

Assume that the number of cochannel signals $L = \mu M$, where M is the number of cells in a cluster and μ is a positive integer. In what follows, the phase shift is disregarded, and the matched filter is tuned to receive

$$y_k(t) = Am_k(t)\cos\left(2\pi f_c t + \beta_k \sin\left(2\pi f_k t\right)\right). \quad (12)$$

Time Domain Analysis. The output of the matched filter at sampling instant t_0 is given by

$$v_k(t_0) = \int_{T_b}\left[\sum_{j=1}^{L}\lambda_j y_j(t)\right]x_k(t)\,dt, \quad (13)$$

where it is assumed that the spatial attenuation factor λ_j is $0 < \lambda_j \ll 1$ for the signals associated with the $M-1$ adjacent cells, and $\lambda_k = 1$ for the μ signals belonging to the home cell. Since $f_c \gg 1/T_b$, then

$$v_k(t) \cong \frac{A^2}{2}m_k(t) + \frac{A^2}{2}\int_{T_b}\sum_{\substack{j=1\\ j\neq k}}^{L}\lambda_j m_j(t) \cdot \cos\left(\beta_k \sin\left(2\pi f_k t\right) - \beta_j \sin\left(2\pi f_j t\right)\right)dt. \quad (14)$$

At the end of every bit interval T_b, the samples $v_k(nT_b)$ are fed into a threshold device with threshold 0 to produce the binary waveform $\widetilde{m}_k(t)$. Consequently, the magnitude of the term on the right hand side should dominate the second term for good performance.

Since $f_i \neq f_k$ and $\beta_i \neq \beta_k$ for $i \neq k$ and $f_i > 1/T_b$ and $\beta_i > 1$ for all i, then the argument corresponding to cos(·) terms can reflect diverse large angles and their cos(·) take on positive and negative values within T_b. The integral of each cos(·) term within T_b becomes ≪1 with either positive or negative values. The summation of small positive and negative values would become significantly smaller than the summation of their magnitudes. The summation of these terms can be thought of as a random walk process. Consequently, as L increases, the performance is expected to degrade.

Frequency Domain Analysis. The Fourier transform of $y_k(t)$ is given by

$$Y_k(f) = \frac{AT_b}{2}\sum_{n=-\infty}^{\infty}J_n(\beta_k) \times \left[\operatorname{sinc}\left(T_b\left(f - f_c - nf_k\right)\right) + \operatorname{sinc}\left(T_b\left(f + f_c + nf_k\right)\right)\right]. \quad (15)$$

As a part of matched-filter reception, the multiplication $y_j y_k$, $1 \leq j \leq L$, in (13) implies the convolution of their spectra in the frequency domain. In order to illustrate the phenomena of rejecting CCI signals, we will examine common spectral bands, particularly, the overlapping of the major part of the sinc functions resulting from matched-filter reception (13) within the bandwidth B with cochannel signals. It is worth noting that $B = 2(\beta_k + 1)f_k = 2(\beta_i + 1)f_i, \forall k, i$, and those spectral components outside B are considered negligible. There are two scenarios that should be examined, in particular, whenever we have

(a) $nf_j = mf_k$ and/or

(b) $|nf_j - mf_k|$ is relatively small with respect to R

for $j \neq k$ and for $|n| = 0, 1, 2, \ldots, \beta_j + 1$, $|m| = 0, 1, 2, \ldots, \beta_k + 1$.

Scenario (a). The associated setting implies that at least one of the "sinc" functions in (15) would entirely overlap, resulting in CCI. That is, if $nf_j = mf_k \Longrightarrow n = m(p_k/p_j)$. Since p_k/p_j is irreducible $\Longrightarrow m = \pm ip_j$, where i is a nonnegative integer, p_j is a prime number, and $ip_j \leq \beta_k$. We have

$$ie < |m| = iR \times l < ip_j \leq \beta_k < \frac{B}{2R} - 1. \quad (16)$$

Since $R \times l$ is constant (Lemma 3) and $ie < iRl < B/2R - 1$ for all values of R, then i can only be equal to zero.

Therefore, the only common spectral component inside B can be the one corresponding to the discrete carrier, which could be made smaller for larger values of β_k (since the envelope of $J_n(\beta_k)$ decreases) or around the zeros of $J_n(\beta_k)$.

Scenario (b). This setting implies that at least one of the "sinc" functions (15) would partly overlap leading also to CCI. Similar to the discussion in the above scenario, we consider $|f_j \pm ip_j f_k|$ to be relatively small with respect to R, where i is a nonnegative integer, p_j is a prime number, and $ip_j \leq \beta_k$. We consider the worst case scenario where $\min_j|f_j - ip_j f_k|$, since $\min_j|f_j - ip_j f_k| \leq |f_j - ip_j f_k| \leq |f_j \pm ip_j f_k|$.

From (7) in Remark 2, $\min_j|f_j - ip_j f_k|$ decreases as γ increases (or spectral efficiency increases) leading to more overlapping spectral bands or worse BER due to SIR. In addition, for a fixed spreading factor α, γ increases as the number of users L increases, which could worsen the performance.

However, for a relatively small value of γ, the significant overlapping band would be at the carrier (Scenario (a)), and a few others may partly overlap depending on the value of γ.

The latter analysis indicates that the proposed scheme is capable of significantly rejecting CCI signals.

4. Numerical Simulations

This section examines the performance of the proposed scheme using numerical simulations. The performance of CIMA is compared with the performance of DSSS-BPSK, since both schemes allow multiple access and require coherent detection. The comparison is based on consistent numerical implementation as far as selecting the relevant parameters. It is important to note that baseband implementation does not exactly match the expected baseband performance when employing the proposed scheme. The reason behind this mismatch is illustrated with the following simple example: If $f_c = 0$, then the frequency separation of the signal doubles;

e.g., the period of $x(t) = A\cos(2\pi f_c t + \beta_m \sin(2\pi f_m t))$ is $1/f_m$; however, the period of $x(t) = A\cos(\beta_m \sin(2\pi f_m t))$ is $1/(2f_m)$ since $\cos(\sin(\pm\alpha)) = \cos(\sin(\alpha))$.

Consequently, the passband approach is implemented for both schemes. The carrier frequency [Hz] in all scenarios is set at $f_c = 8\alpha R$, and the sampling frequency [Hz] at $f_s = 8(f_c + \alpha R)$, where α and R are the spreading factor and the bit rate for both CIMA and DSSS-BPSK. For consistency, we select the chip period, employed in DSSS-BPSK, to be equal to $1/(\alpha R)$. The Mersenne Twister PRNG, which is used as the default stream at MATLAB startup and several other software systems, is adopted for generating the codes associated with DSSS-BPSK. Although it is the most widely used PRNG [32], the codes generated by Mersenne Twister have finite correlation values for other than zero delay. MATLAB was employed to carry out all the simulations.

In what follows, we first examine the PSD and the bandwidth of three CIMA signals to further illustrate the frequency interleaving CIMA employs. Next, we compute the BER due to channel noise, with and without multipath channel consideration, and cochannel interference (CCI) for CIMA and DSSS-BPSK. Several plots have been presented to encompass all aspects of CIMA performance by varying the spreading factor, spectral efficiency, and signal-to-interference ratio (SIR) of CCI signals. All simulations are done on passband signals with a bit rate of $R = 20$ bits/s and with f_c and f_s as defined above.

4.1. CIMA PSD and Bandwidth. This part examines the single-sided spectrum and bandwidth of three CIMA signals. The purpose of this study is not meant to evaluate the performance of the proposed algorithm but only to illustrate the relevant analytical work including (10).

The employed spreading factor is $\alpha = 100$ and the spectral efficiency $\gamma = 0.3$ bits/sec/Hz. Following from (10) in Section 3, the null-to-null bandwidth $B_y \cong (\alpha + 2)R = 2040$ Hz $\approx B = \alpha R = 2000$ Hz. β_j and f_j are chosen such that $2(\beta_j + 1)f_j = B = 2000$ Hz, for $j = 1, 2$, or 3. Examining Figure 2, we notice that no significant power occurs beyond 1020 Hz, which confirms (10). In addition, as discussed in Section 3.3 (frequency domain analysis), the only completely overlapping "sinc" function is at the carrier (Scenario (a)) and few others partly overlap. The spectrum holes are due to the employed relatively large spreading factor for only three users.

4.2. AWGN and Multipath Fading Channel. The performance of CIMA and DSSS-BPSK in the presence of an additive white Gaussian noise (AWGN) channel is examined in this part of the simulations. Simulations for one and seven users under AWGN and multipath fading channel are carried out. A spreading factor of $\alpha = 60$ is considered for both modulation schemes. The BER versus E_b/N_0 in the AWGN with no multipath channel for both schemes is shown in Figure 3, where E_b/N_0 ranges from −1 to 9 dB in increments of 1 dB. It is important to note that single-user CIMA and DSSS-BSPK perform similarly to BPSK. For seven users, the proposed method outperforms DSSS-BPSK under consideration. Based on numerical simulations, the DSSS-BPSK BER

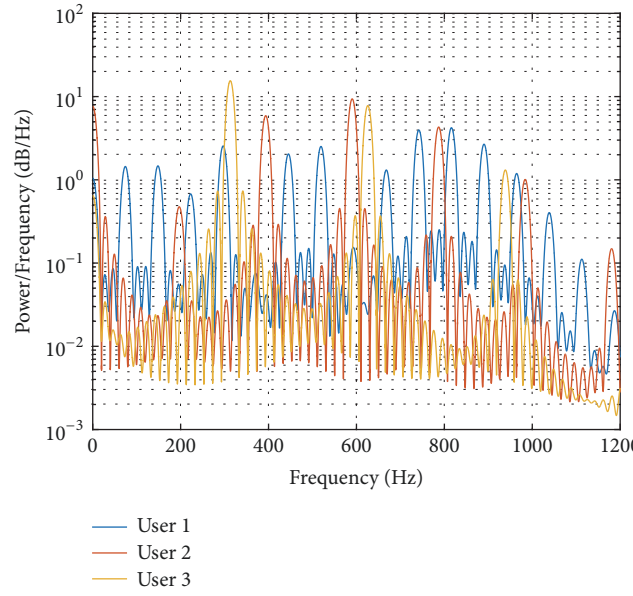

Figure 2: Power spectral density of 3 CIMA signals with corresponding PRNG parameter pairs: $\beta_1 = 12.4783$, $f_1 = 74.1935$ Hz. $\beta_2 = 4.0820$, $f_2 = 196.7742$ Hz. $\beta_3 = 2.1959$, $f_3 = 312.9032$ Hz.

using Mersenne Twister PRNG, in presence of AWGN (e.g., $\alpha = 60$ and $L = 7$), can be closely approximated by the analytical model of DSSS-BPSK, which is given by

$$\text{BER} = Q\left[\frac{1}{\sqrt{(L-1)/\alpha + N_0/2E_b}}\right]. \quad (17)$$

However, the performance of DSSS-BPSK should be generally affected by the nonzero correlation among the random spreading codes generated by the Mersenne Twister PRNG.

In order to further demonstrate the potential of the proposed scheme, a simulation in a multipath fading channel is depicted in Figure 4. Four taps with relative path gains of 0 dB, -3 dB, -6 dB, and -9 dB and uniformly distributed random path delays between T_{cp} and $3T_{cp}$ are considered for the multipath fading channel, where $T_{cp} = 1/\alpha R$ is the DSSS-BPSK chip period. The results in Figure 4 show that the performance of CIMA and DSSS degrades in a multipath channel, with CIMA still performing similarly to DSSS in single-user application and better with seven users.

4.3. Cochannel Interference. Since both schemes allow multiple access, it is important to assess their performance in function of the spreading factor for a specific number of users. We examine the BER in function of the spreading factor for a fixed number of users. This implies that as the spreading factor increases, the spreading bandwidth increases, and subsequently the spectral efficiency decreases. Figure 5 shows the BER for different spreading factors. The number of users is set to 10 for both CIMA and DSSS. The spreading factor is varied from 10 to 60. It is important to note that the product $\gamma\alpha = L$ was held constant in the case of CIMA, where L is the number of users sharing the same channel. Figure 5 shows the BER for different spreading factors. As

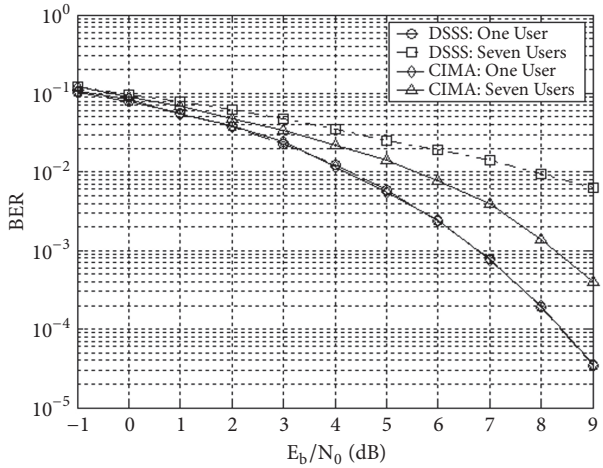

Figure 3: BER versus E_b/N_0 of CIMA and DSSS-BPSK in an AWGN channel for 1 and 7 users and $\alpha = 60$.

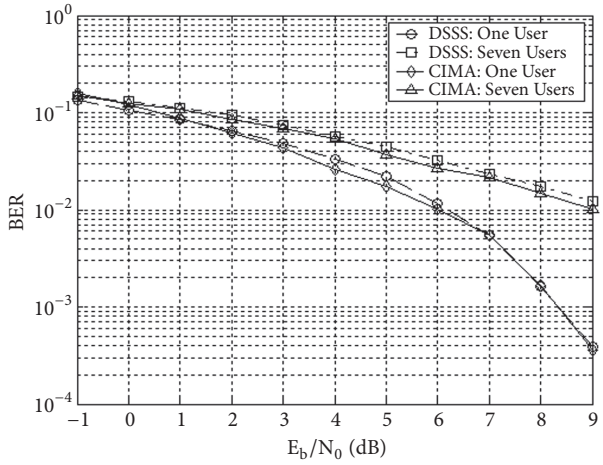

Figure 4: BER versus E_b/N_0 of CIMA and DSSS-BPSK in an AWGN with a four-tap multipath channel for 1 and 7 users and $\alpha = 60$.

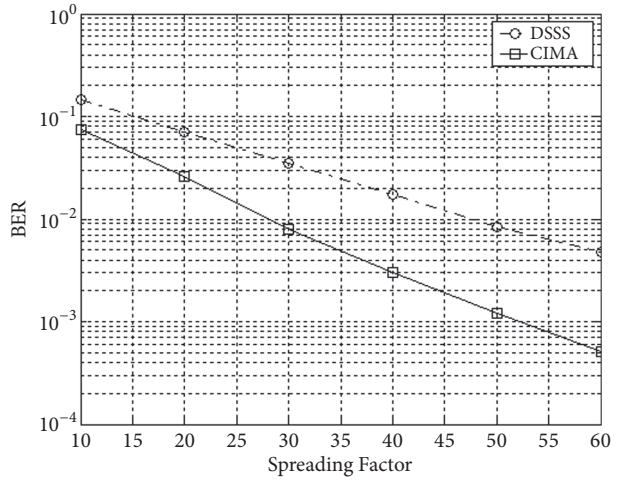

Figure 5: BER versus the spreading factor α for CIMA and DSSS-BPSK for 10 users.

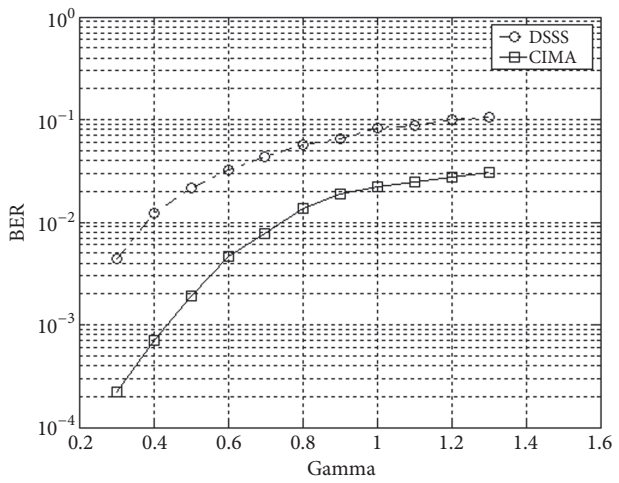

Figure 6: BER versus the spectral efficiency γ for CIMA and DSSS-BPSK for spreading factor $\alpha = 100$ and the number of users varied from 30 to 130.

expected, the performance of both schemes improves as the spreading factor increases, since the spreading bandwidth is also increasing.

4.4. Spectral Efficiency. We compare the performance of CIMA with DSSS-BPSK in terms of the spectral efficiency. Contrary to the previous scenario, we look at how the BER is affected by the number of users when the spreading factor is fixed. Figure 6 presents the BER while varying the values of γ, where $\gamma = L/\alpha$, $\alpha = 100$, and L is the number of users ranging from 30 to 130. The power of each cochannel interferer is 50% of the targeted signal power. The resulting BER in Figure 6 shows that performance of both CIMA and DSSS-BPSK degrades as the spectral efficiency increases, which is expected since more users are accessing the channel. It follows directly from Figure 6 that CIMA performs better than DSSS for all spectral efficiencies. It is important to note that the BER pertaining to CIMA at a 130% spectral efficiency is about three times smaller than the corresponding BER associated with DSSS-BPSK, which further affirms the potential of the proposed scheme.

4.5. Signal-to-Interference Ratio. The performance of both schemes for different signal-to-interference ratios (SIRs) is also evaluated at a 100% spectral efficiency. The transmitted signal power to the total interfering signals' power ratio is varied from -10 dB to 0 dB. In order to achieve such SIR variations, we are artificially changing the transmitted power of users to modify the power ratio between the user of interest and other users. The total interfering signal power is considered to be the sum of the powers of individual interferers. A spreading factor of 10 and a number of 10 users are considered for this part of the simulation. The BER curves are shown in Figure 7. It is also evident that CIMA performs better than DSSS-BPSK for all SIRs, with an acceptable performance at -10 dB and a BER almost 35 times smaller than DSSS-BPSK at 0 dB.

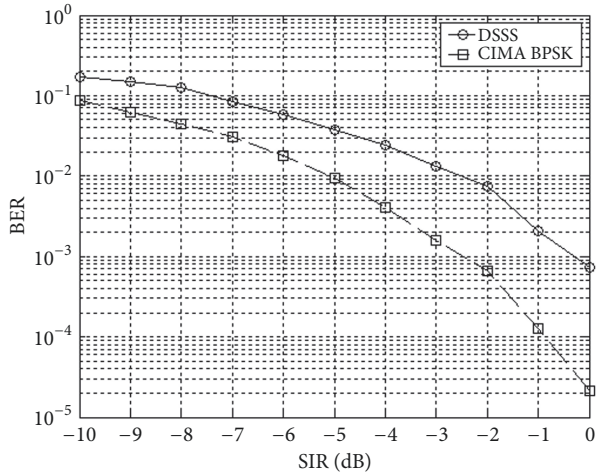

Figure 7: BER versus SIR for CIMA and DSSS-BPSK for 10 users and spreading factor $\alpha = 10$.

5. Conclusion

In this paper a novel multiple-access modulation scheme was proposed that employs a nontraditional PRNG. The system provided a capability of significantly rejecting cochannel and adjacent channel interference. Based on numerical simulations, CIMA performance in the presence of channel noise was shown to be similar to DSSS-BPSK with orthogonal spreading codes. In addition, CIMA outperforms DSSS-BPSK using Mersenne Twister PRNG, in the case of multipath delay with multiple users, CCI, spectral efficiency, and SIR. This work unlocked the door for consideration of other modulation schemes in employing the nontraditional PRNG proposed in [30]. Future works may include the use of a Gaussian filter along with an equalizer integrated with CIMA to reduce the effects of intersymbol interference caused by the Gaussian filter on the modulating data. Using the appropriate equalizer can further improve the performance of CIMA in the presence of noise and cochannel interference.

Appendix

In the following, we present three propositions that help in establishing further characteristics pertaining to CIMA.

Proposition A.1. *The number of prime numbers generated by the proposed algorithm is given by*

$$L \cong \int_{p_{\min}}^{p_{\max}} \frac{d\sigma}{\ln(\sigma)}. \tag{A.1}$$

Proof. The proof can be readily deduced from fact that the number of prime numbers below a given number, n, is well approximated by the offset logarithmic integral given by

$$\mathrm{Li}(n) = \int_2^n \frac{d\sigma}{\ln(\sigma)}. \tag{A.2}$$

□

Proposition A.2. *l increases if and only if L increases.*

Proof. Necessary condition: This can be verified by considering the following:

$$\begin{aligned}\frac{d}{dl}L &\cong \frac{d}{dl}\int_{p_{\min}}^{p_{\max}} \frac{d\sigma}{\ln(\sigma)} \\ &= \frac{dp_{\max}}{\ln(p_{\max})} - \frac{dp_{\min}}{dl}\frac{1}{\ln(p_{\min})} \\ &\cong \frac{B}{2(\beta_{\min}+1)}\frac{1}{\ln(lb/2(\beta_{\min}+1))} - R\frac{1}{\ln(lR)}.\end{aligned} \tag{A.3}$$

Note $(d/dz)(z/\ln(lz)) = (\ln(lz)-1)/(\ln(lz))^2 > 0, lz > e$

since $p_{\max} = Bl/2(\beta_{\min}+1) > p_{\min} \geq Rl > e \Longrightarrow dL/dl > 0$.

Consequently, as l increases, L increases.

Sufficient condition: Let $g(\cdot)$ be the function such that $L = g(l)$. Since L is a continuous (and differentiable) function and $g(\cdot)$ is a strictly increasing function over the specified domain, then $g^{-1}(\cdot)$ exists where $l = g^{-1}(L)$, and $g^{-1}(\cdot)$ is continuous and strictly increasing; hence as L increases, l increases. □

Proof of Lemma 3. The proof is conducted using a contradiction argument. Based on Proposition A.1, L can be presented as

$$L = g(z_1) = \int_{z_1}^{cz_1} \frac{d\sigma}{\ln(\sigma)}, \tag{A.4}$$

where $z_1 \equiv R \times l > e$ and $c \equiv \alpha/2(\beta_{\min}+1) > 1$.

$L = \gamma\alpha$ is fixed; assume there exists $z_2 \neq z_1$, where $z_2 > e$, such that

$$L = \int_{z_2}^{cz_2} \frac{d\sigma}{\ln(\sigma)} \Longrightarrow \frac{dL}{dc} = \frac{z_2}{\ln(cz_2)}. \tag{A.5}$$

However, since $c > 1$ and $cz > e$, $z/\ln(cz)$ is a strictly increasing function. Therefore, for $z_1 \neq z_2$, it leads to $L \neq L$, which leads to a contradiction. Consequently, the product $R \times l$ is constant. □

Corollary A.3. *Assume $f_c \gg R$; then $\{\beta_j\}$ and BER are independent of R for fixed values of γ and α where $\alpha > 2(\beta_{\min}+1)$ and $\gamma > 0$.*

Proof. From Lemma 3, the product Rl is constant and independent of R for fixed values of γ and α. Consequently, the lower and upper bound of the prime numbers p_j are independent of R; hence $\{p_j\}$ is a set of values independent of R. Since $\beta_j = lB/2p_j - 1 = \alpha lR/2p_j - 1$, $\forall j \Longrightarrow \{\beta_j\}$ is a set of values independent of R. Consider $f_j = B/2(\beta_j+1) = (\alpha/2(\beta_j+1))R$.

Therefore, the output of the corresponding matched filer (14) yields

$$\begin{aligned}v_k(t) \cong \frac{A^2}{2}m_k(t) + \frac{A^2}{2}\int_1 \sum_{\substack{j=1 \\ j\neq k}}^{L} \lambda_j m_j(t) \\ \cdot \cos\left(\beta_k \sin\left(\frac{\pi\alpha t}{\beta_k+1}\right) - \beta_j \sin\left(\frac{\pi\alpha t}{\beta_j+1}\right)\right) dt.\end{aligned} \tag{A.6}$$

Since the output of the matched filter is independent of R and f_c so is the output of the receiver and hence the BER. □

A Proposed Approach for Generating f_i and β_i

The inputs of a code that generates different pairs (β_i, f_i) can be the spreading factor α, the spectral efficiency γ, and the bit rate R (and β_{min} is set to a constant, e.g., $\beta_{min} = 1.2$). Consequently, the spread bandwidth becomes $B = \alpha R$. The bounds for p_j become $Rl \leq p_j \leq Bl/2(\beta_{\min} + 1),\ 1 \leq j \leq L$.

In order to find a sufficiently large value of l corresponding to the desired value of $L = \alpha\gamma$ (desired number of users), it is recommended to start at $3/R$ (in order to guarantee that $Rl > e$) and keep on increasing l (e.g., while loop) until L prime numbers are generated.

Set: $f_j \equiv p_j/l,\ 1 \leq j \leq L$, and $\beta_j \equiv B/2f_j - 1, 1 \leq j \leq L$.

Data Availability

The data can be easily generated by using the model provided in the manuscript.

Conflicts of Interest

The authors declare that they have no conflicts of interest.

Acknowledgments

The authors would like to thank Mr. Michel Nacouzi for conducting helpful numerical simulations relevant to CIMA, which are not shown in this manuscript. The authors would also like to thank the anonymous reviewers for their helpful comments.

References

[1] D. Evans, *The Internet of Things: How the Next Evolution of the Internet is Changing Everything*, Cisco Internet Business Solutions Group, April 2011.

[2] K. David, D. Dixit, and N. Jefferies, "2020 Vision," *IEEE Vehicular Technology Magazine*, vol. 5, no. 3, pp. 22–29, 2010.

[3] S. Kondo and B. Milstein, "Performance of multicarrier DS CDMA systems," *IEEE Transactions on Communications*, vol. 44, no. 2, pp. 238–246.

[4] B. Yu, Y. Bao, H. Wei, X. Huang, and Y. Shu, "Collaborative covert communication design based on lattice reduction aided multiple user detection method," *Wireless Communications and Mobile Computing*, vol. 2017, Article ID 8949430, 8 pages, 2017.

[5] L. Nguyen, "Self-encoded spread spectrum communications," in *Proceedings of the Conference on Military Communications (MILCOM'99)*, pp. 182–186, Atlantic City, NJ, USA.

[6] K. Siwiak, "Ultra-wide band radio: Introducing a new technology," in *Proceedings of the IEEE VTS 53rd Vehicular Technology Conference (VTS SPRING 2001)*, pp. 1088–1093, Greece, May 2001.

[7] Y.-R. Tsai and X.-S. Li, "Kasami code-shift-keying modulation for ultra-wideband communication systems," *IEEE Transactions on Communications*, vol. 55, no. 6, pp. 1242–1252, 2007.

[8] G. Kaddoum, F.-D. Richardson, and F. Gagnon, "Design and analysis of a multi-carrier differential chaos shift keying communication system," *IEEE Transactions on Communications*, vol. 61, no. 8, pp. 3281–3291, 2013.

[9] M. K. Patel, S. M. Berber, and K. Sowerby, "Antijamming performance of adaptive chaos based CDMA system with MRC in imperfect channel estimation environment," *Wireless Communications and Mobile Computing*, vol. 2017, Article ID 2716949, 5 pages, 2017.

[10] M. Herceg, G. Kaddoum, D. Vranjes, and E. Soujeri, "Permutation index DCSK modulation technique for secure multiuser high-data-rate communication systems," *IEEE Transactions on Vehicular Technology*, vol. 67, no. 4, pp. 2997–3007, 2018.

[11] M. Herceg, D. Vranjes, G. Kaddoum, and E. Soujeri, "Commutation Code Index DCSK Modulation Technique for High-Data-Rate Communication Systems," *IEEE Transactions on Circuits and Systems II: Express Briefs*, 2018.

[12] G. Kaddoum, Y. Nijsure, and H. Tran, "Generalized code index modulation technique for high-data-rate communication systems," *IEEE Transactions on Vehicular Technology*, vol. 65, no. 9, pp. 7000–7009, 2016.

[13] A. Cassola, T. Jin, G. Noubir, and B. Thapa, "Efficient spread spectrum communication without preshared secrets," *IEEE Transactions on Mobile Computing*, vol. 12, no. 8, pp. 1669–1680, 2013.

[14] W. D. Lane and A. M. Bush, "Spread-spectrum multi-h modulation," *IEEE Journal on Selected Areas in Communications*, vol. 8, no. 5, pp. 728–742, 1990.

[15] F. Giannetti, M. Luise, and R. Reggiannini, "Continuous-Phase Modulations for CDMA Radio Communications: Modem Architecture and Performance," *European Transactions on Telecommunications*, vol. 7, no. 3, pp. 225–233, 1996.

[16] R. T. Hsu and J. S. Lehnert, "The performance of continuous-phase-coded DS/SSMA communications," *IEEE Transactions on Communications*, vol. 46, no. 4, pp. 533–543, 1998.

[17] F. Yang, S. H. Leung, C. Y. Ngan, and G. Bi, "The performance and design criterion of phase spreading sequences for DS/SSMA communications with full response CPM over Rayleigh fading channels," in *Proceedings of the IEEE Global Telecommun Conference - GLOBECOM'99*, vol. 1B, pp. 914–918, December 1999.

[18] A. T. McDowell, J. S. Lehnert, and Y. K. Jeong, "Dual-phase continuous phase modulation for spread-spectrum multiple-access communication," *IEEE Transactions on Communications*, vol. 52, no. 5, pp. 823–833, 2004.

[19] E. Soujeri, G. Kaddoum, and M. Herceg, "Design of an initial condition-index chaos shift keying modulation," *IEEE Electronics Letters*, vol. 54, no. 7, pp. 447–449, 2018.

[20] P. Som and A. Chockalingam, "Performance analysis of space-shift keying in decode-And-forward Multihop MIMO networks," *IEEE Transactions on Vehicular Technology*, vol. 64, no. 1, pp. 132–146, 2015.

[21] X. Li, S. Hong, V. D. Chakravarthy, M. Temple, and Z. Wu, "Intercarrier interference immune single carrier OFDM via magnitude-keyed modulation for high speed aerial vehicle communication," *IEEE Transactions on Communications*, vol. 61, no. 2, pp. 658–668, 2013.

[22] S. Vaughan-Nichols, "OFDM: back to the wireless future," *The Computer Journal*, vol. 35, no. 12, pp. 19–21, 2002.

[23] E. Soujeri, G. Kaddoum, M. Au, and M. Herceg, "Frequency Index Modulation for Low Complexity Low Energy Communication Networks," *IEEE Access*, vol. 5, pp. 23276–23287, 2017.

[24] R. L. Peterson, R. E. Ziemer, and E. David, *Introduction to Spread Spectrum Communications*, Prentice Hall, Englewood Cliffs, NJ, USA, 1995.

[25] R. Gold and R. Dixon, "Method and Apparatus for Despreading Spread Spectrum Signals," *Patent Number*, vol. 5, pp. 761-239, 1998.

[26] T. Kasami, "Weight distribution formula for some class of cyclic codes," Defense Technical Information Center R-285(AD 632574), Coordinated Science Lab., Univ., Urbana, Ill, USA, 1966.

[27] R. H. Barker and R. H, "Group Synchronizing of Binary Digital Sequences," in *Communication Theory*, pp. 273–287, Butterworth, London, 1953.

[28] V. Tarokh, H. Jafarkhani, and A. R. Calderbank, "Space-time block codes from orthogonal designs," *IEEE Transactions on Information Theory*, vol. 45, no. 5, pp. 1456–1467, 1999.

[29] V. Tarokh, N. Seshadri, and A. R. Calderbank, "Space-time codes for high data rate wireless communication: performance criterion and code construction," *IEEE Transactions on Information Theory*, vol. 44, no. 2, pp. 744–765, 1998.

[30] S. S. Saab, J. G. Hobeika, and I. E. Ouaiss, "A novel pseudo-random noise and band jammer generator using a composite sinusoidal function," *IEEE Transactions on Signal Processing*, vol. 58, no. 2, pp. 535–543, 2010.

[31] J. Gu, W. S. Jeon, and J. M. Kim, "Proactive frequency-hopping dynamic spectrum access against asynchronous interchannel spectrum sensing," *IEEE Transactions on Vehicular Technology*, vol. 62, no. 8, pp. 3614–3626, 2013.

[32] S. Marsland, *Machine Learning: An Algorithmic Perspective*, CRC Press, 2011.